eIF3i promotes colorectal cancer cell survival *via* augmenting PHGDH translation

Yaguang Zhang[1,2,‡], **Xiaowen Wan**[1,‡], **Xuyang Yang**[1,2], **Xueqin Liu**[1], **Qing Huang**[1], **Lian Zhou**[1], **Su Zhang**[1], **Sicheng Liu**[1], **Qunli Xiong**[2], **Mingtian Wei**[2], **Lei Qiu**[1,2], **Bo Zhang**[2], and **Junhong Han**[1,2,*]

From the [1]Department of Biotherapy, Cancer Center and State Laboratory of Biotherapy, and Frontiers Science Center for Disease-related Molecular Network, and [2]Research Laboratory of Cancer Epigenetics and Genomics, Department of General Surgery, Frontiers Science Center for Disease-related Molecular Network, West China Hospital, Sichuan University, Chengdu, China

Reviewed by members of the JBC Editorial Board. Edited by Eric Fearon

Translational regulation is one of the decisive steps in gene expression, and its dysregulation is closely related to tumorigenesis. Eukaryotic translation initiation factor 3 subunit i (eIF3i) promotes tumor growth by selectively regulating gene translation, but the underlying mechanisms are largely unknown. Here, we show that eIF3i is significantly increased in colorectal cancer (CRC) and reinforces the proliferation of CRC cells. Using ribosome profiling and proteomics analysis, several genes regulated by eIF3i at the translation level were identified, including D-3-phosphoglycerate dehydrogenase (PHGDH), a rate-limiting enzyme in the *de novo* serine synthesis pathway that participates in metabolic reprogramming of tumor cells. PHGDH knockdown significantly represses CRC cell proliferation and partially attenuates the excessive growth induced by *eIF3i* overexpression. Mechanistically, METTL3-mediated N6-methyladenosine modification on PHGDH mRNA promotes its binding with eIF3i, ultimately leading to a higher translational rate. In addition, knocking down *eIF3i* and *PHGDH* impedes tumor growth *in vivo*. Collectively, this study not only uncovered a novel regulatory mechanism for PHGDH translation but also demonstrated that eIF3i is a critical metabolic regulator in human cancer.

Colorectal cancer (CRC) is a common type of malignant tumor in the gastrointestinal system. CRC ranks third among newly diagnosed cancers (11.4% of total cases), following female breast cancer (11.7%) and lung cancer (11.4%) (1). Most patients with early-stage CRC can obtain a favorable prognosis through surgical treatment (2). However, most diagnosed cases of CRC are at an advanced stage, the therapeutic efficacy is insufficient, resulting in a high mortality rate (3). CRC mortality (9.4%) has ascended to the second place among cancers worldwide, and the number of patients continues to rise (1). Therefore, it is necessary to explore the molecular mechanisms of CRC occurrence and development for screening and identifying new cancer markers or drug targets.

The major carrier of life activities is protein and its synthesis is controlled by translation initiation factors and post-transcriptional modifications. Abnormal protein synthesis leads to abnormal gene expression, resulting in aberrant cell proliferation, which is a key factor accounting for tumor development and metastasis (4–6). The most frequent internal modification on mammalian messenger RNA is N6-methyladenosine (m6A), which affects RNA stability, splicing, nuclear export, and translation *via* m6A-specific binding proteins (7–9). Increasing evidence indicates that m6A modification of some target genes has diverse roles in tumorigenesis. Jin *et al.* discovered that methyltransferase-like protein 3 (METTL3) played a crucial role in the m6A modification of YAP, contributing to drug resistance and metastasis in non-small cell lung cancer (10). They also found that YT521-B homology domain family 1/3 (YTHDF1, YTHDF3) and eukaryotic translation initiation factor 3 subunit b promoted YAP translation by directly interacting with m6A-modified YAP mRNA. Additionally, there were reports demonstrated that METTL3 catalyzed the m6A modification of Snail, facilitating YTHDF1-mediated translation, and influencing the process of epithelial-mesenchymal transition in hepatocellular carcinoma (HCC) cells (11). Furthermore, a separate finding indicated that β-catenin suppressed the production of miR455-3p and activated METTL3, leading to increased m6A modification of heat shock transcription factor 1 and enhancing its translation efficiency. This mechanism promoted the development of one mutated copy of the adenomatous polyposis coli (Apc) gene, which prones to developing multiple intestinal neoplasia (min) (APC^min/+) colorectal cancer (12). Recent investigations have demonstrated that N-acetyltransferase 10-mediated acetylation of cytidine (ac4C) in mRNA amplifies translation efficiency and facilitates tumor cell proliferation and migration (13–15). However, the regulation of mRNA modification and function of RNA-binding proteins, particularly in relation to translation initiation factors and their impact on protein synthesis, remains largely unknown.

Eukaryotic translation initiation factor 3 subunit i (eIF3i) is one of the 13 subunits of the mammalian eIF3 complex, which can interact with the ribosomal subunit 40S to stimulate the formation of the 43S precursor initiation complex (16).

Emerging evidence showed that eIF3i were upexpressed in various cancers, including colon adenocarcinoma, HCC, head and neck squamous cell carcinoma. and melanoma (17–20). Thus, eIF3i was considered a proto-oncogene that promoted cell proliferation and tumorigenesis by regulating protein synthesis (21). Our previous studies have shown that eIF3i is upregulated in the liver, blood vessels, and intestinal tissues of early zebrafish embryos and modulates vascular cell response to tumor signals and angiogenesis by regulating the translation of vascular endothelial growth factor (VEGF) and vascular endothelial growth factor receptor 2 (18, 22). However, the target genes regulated by eIF3i in CRC are still elusive.

Phosphoglycerate dehydrogenase (PHGDH) is a key rate-limiting enzyme in the serine synthesis pathway, which catalyzes the oxidation of 3-phosphoglycerate produced from glycolysis to 3-phosphohydroxypyruvate (23). PHGDH provides the one-carbon monomer required for the *de novo* synthesis of purine and deoxythymidine *via* the serine synthesis pathway (24). In addition, PHGDH which is phosphorylated by PKCζ inhibits its enzymatic activity, and loss of PKCζ in tumor cells boosts the plasticity of metabolic reprogramming in the absence of glucose through glutamine consumption by the serine synthesis pathway (25). The involvement of PHGDH in tumor growth and resistance has also been found through the serine synthesis pathway, including breast cancer, melanoma, and HCC (26–29). Patients with high PHGDH expression have poor prognosis, suggesting that PHGDH may serve as an independent predictor of poor prognosis in CRC (30). However, key factors that regulates PHGDH translation and its role in CRC development remain unclear. In this study, we systematically examined the expression of eIF3i and PHGDH and explored their roles in CRC cell survival through both *in vitro* and *in vivo* experiments. More importantly, the underlying molecular mechanisms were investigated in depth, and we found that eIF3i regulated PHGDH translation efficiency in an m^6A-dependent manner in CRC cells. This is particularly relevant in light of the findings (25). Taken together, our findings suggested that eIF3i plays a critical role in the metabolic cascade in tumorigenesis.

Results

eIF3i is remarkably upregulated in CRC

Our previous research found that eIF3i was highly expressed in the early development of zebrafish embryos, including the intestine, *via* an in situ hybridization assay (18). As embryonic development and tumorigenesis shared many molecular mechanisms (31), we speculate that eIF3i may play an important role in the occurrence and development of CRC.

To test this hypothesis, we detected the expression of eIF3i in clinical CRC samples using the Human Protein Atlas database. As shown in Figure 1A, we found that eIF3i is significantly overexpressed in CRC (median: 153.4 fragments per kilobase million). We then compared the expression of eIF3i in normal and cancer tissues *via* TIMER2 database and found that eIF3i was markedly upregulated in many cancer types, including bladder urothelial carcinoma, breast invasive

carcinoma, esophageal carcinoma, cholangio carcinoma, colon adenocarcinoma *et al* (Fig. 1B). Furthermore, data analysis from The Cancer Genome Atlas (TCGA) cohort and GSE32323 cohort indicated that eIF3i expression was notably elevated in CRC tissues compared to healthy tissues (Figs. 1C and S1A), but eIF3i expression was not significantly correlated with the tumor grade of CRC (Fig. S1B). We then collected paracancerous and tumor tissues from six CRC patients. Both real-time quantitative polymerase chain reaction (RT-qPCR) and Western blot results showed that eIF3i was highly expressed in tumor tissues compared to paracancerous tissues (Fig. 1, D and E). These results are consistent with the immunohistochemistry (IHC) results (Figs. 1F and S1, C and D).

In addition, we investigated the genetic alteration of eIF3i in COAD cohort and found that the frequency of eIF3i alteration in CRC is 7%, including deletion and mutation (Fig. S1E). A K185N mutation in WD40 domain of eIF3i was observed, which was a potential acetylation and ubiquitination modification site in eIF3i (Fig. S1F). The expression of eIF3i was found to be associated with different types of copy number alterations including deep deletion, shallow deletion, and diploid states. Patients with shallow deletions showed reduced levels of eIF3i (Fig. S1G). Further, CRC patients with genetic alterations were mainly distributed in stage III (71.43%) (Fig. S1H). Additionally, it was observed that genetic alterations were not associated with a better prognosis, as depicted in Fig. S1I. Taken together, these results demonstrate a critical role of eIF3i in CRC progression.

eIF3i promotes the proliferation of CRC cells *in vitro*

Similar to the results presented in patients, we observed high eIF3i expression in CRC cell lines compared to normal intestinal epithelial cell line NCM460 (Fig. 2A). Our findings indicate that eIF3i is predominantly localized in the cytoplasm, as determined by immunofluorescence (Fig. S2, A and B). When *eIF3i* was knocked down by shRNA (Fig. 2B), the proliferation of HCT116 and HT29 cells was markedly inhibited (Fig. 2, C–E). This phenomenon was also confirmed by data obtained from the EdU incorporation assay, which provides a sensitive and robust method to detect and quantify cell proliferation (Fig. 2, F and G). In addition, we found that loss of eIF3i induced apoptosis in HCT116 and HT29 cells detected by flow cytometry (Fig. S2, C–F). Together, these results imply the critical role of eIF3i in both CRC cell proliferation and apoptosis.

Identification of target genes translationally regulated by eIF3i

To identify potential eIF3i translational–regulated genes in CRC, we employed RNA-seq, ribosome profiling (Ribo-seq) and proteomics approaches. RNA-seq results showed that *eIF3i* knockdown resulted in 224 genes downregulation and 161 genes upregulation, while 15,184 genes remained stable (Fig. S3A). Gene Ontology assay showed that differentially expressed genes (DEG) were primarily involved in the
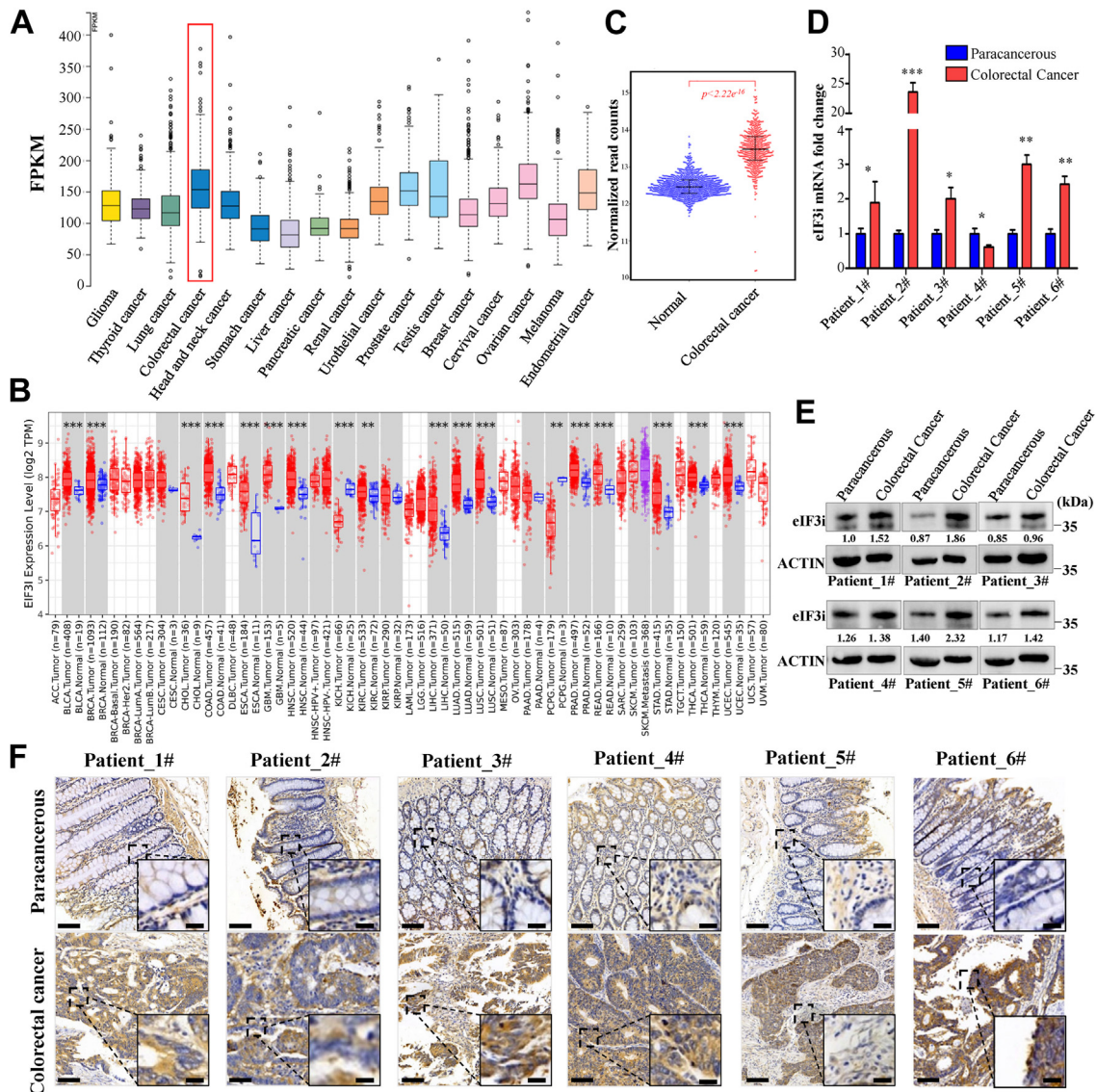
Figure 1. eIF3i is significantly upregulated in CRC. *A*, RNA expression of eIF3i in various tumors from the Human Protein Atlas dataset. *B*, RNA expression of eIF3i in various normal and tumor tissues from TIMER2.0 database, which is an ideal resource for the systematic analysis of associations between gene expression and tumor features in TCGA. *C*, RNA expression of eIF3i in normal and CRC from TCGA and genotype-tissue expression datasets. *D*, analysis of eIF3i expression levels between normal tissues and colorectal cancer tissues. Data represent mean ± SD. Significance of expression level differences was determined using Student's *t* test. *$p < 0.05$; **$p < 0.01$; and ***$p < 0.001$. *E*, Western blot analysis of eIF3i protein expression in paracancerous and cancer tissues from CRC patients. *F*, representative IHC detection of eIF3i in human colorectal cancer and paracancerous tissue. A higher magnification of a representative eIF3i-positive microglia is shown in the *lower right corner*. *Brown stained* for positive cells. The scale bar in *left* represents 100 μm; the scale bar in *right* represents 20 μm. eIF3i, eukaryotic translation initiation factor 3 subunit i; FPKM, fragments per kilobase million; IHC, immunohistochemistry; TCGA, The Cancer Genome Atlas.

development of blood vessel and large ribosome subunit biogenesis (Fig. S3*B*). Ribo-seq is a technique that utilizes deep sequencing to analyze ribosome-protected mRNA fragments. This approach captures a comprehensive view of ribosomes that are actively engaged in translation within a specific time frame. This information can help researchers determine which proteins are being actively translated in a cell. Statistics of clean reads from Ribo-seq in each sample showed that the length of ribosome-protected RNA fragments was about 25 to 32 nt (Fig. S3*C*), and mainly distributed in the coding sequence region of the genome (Fig. S3*D*). Ribo-seq screened 1470 genes with ribosome binding, including 464 genes with reduced binding and 271 genes with increased binding, and 14,023

genes showed no change after *eIF3i* knockdown (Fig. S3*E*). In addition, the Gene Ontology assay showed that differentially expressed genes participates in biological processes, such as gene transcription, translation metabolic, and biosynthetic (Fig. S3*F* and Table S1). And these genes are involved in viral infection, cholesterol metabolism, and amino acids biosynthesis (Fig. S3*G* and Table S2). The analysis of the P site and ORF using Ribo-seq revealed that knockdown of *eIF3i* led to an increase in the proportion of P site occupancy from 28 to 30 nt reads (shNT: 65.01%; sheIF3i: 70.38%) (Fig. S3*H*). Additionally, there was an increase in the number of upstream ORFs (uORFs) (shNT: 59; sheIF3i: 78) (Fig. S3*I*). Both the P site and uORF play regulatory roles in eukaryotic gene
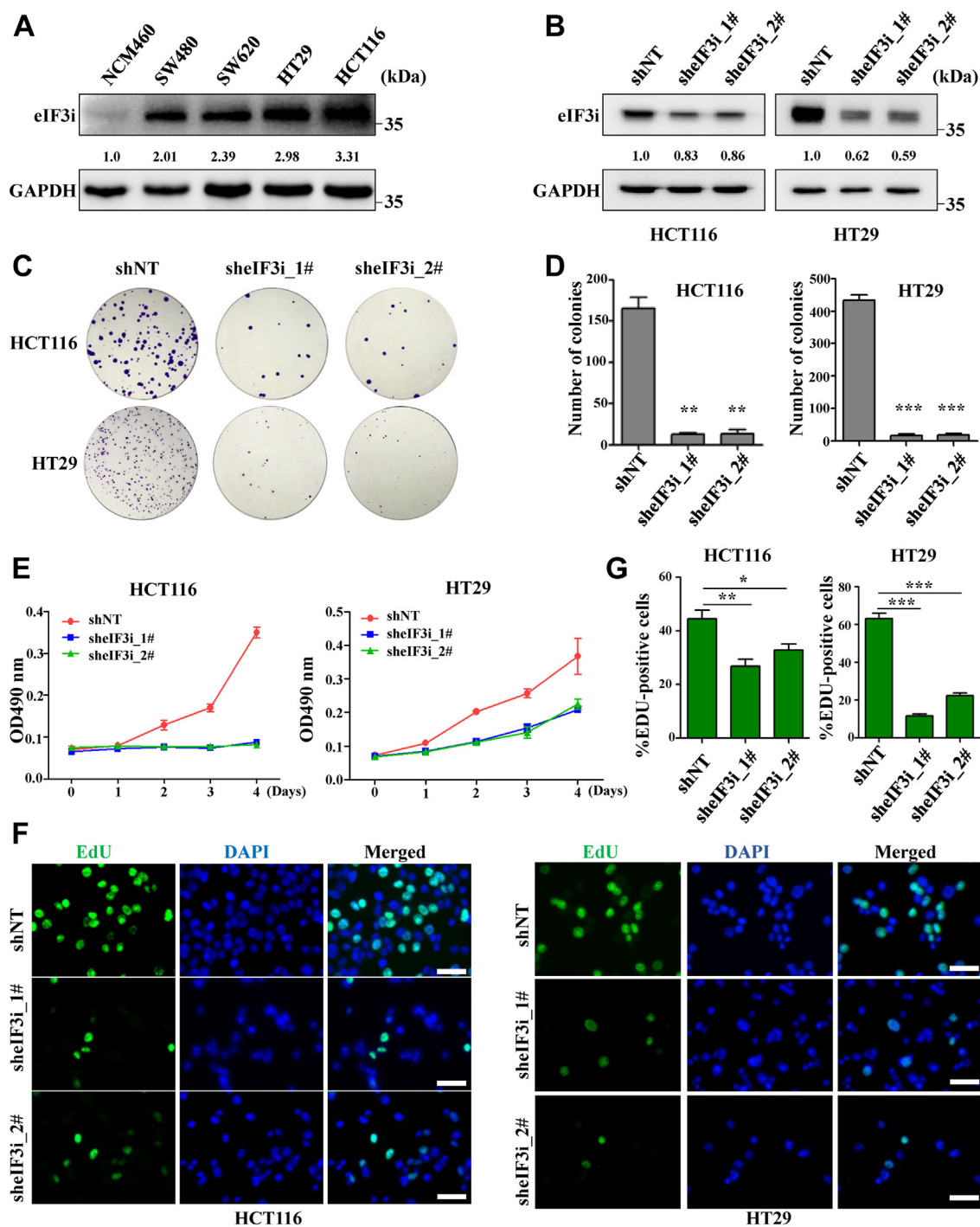
Figure 2. Knocking down eIF3i inhibited cell proliferation. *A*, Western blotting was used to detect eIF3i expression in NCM460, SW480, SW620, HT29, and HCT116 cells. *B*. Western blotting was used to detect the knockdown efficiency of eIF3i-shRNA in HCT116 and HT29 cells. shNT, cells transfected with scrambled shRNA. sheIF3i, cells transfected with eIF3i shRNA. *C* and *D*, cell proliferation of HCT116 and HT29 cells with or without eIF3i depletion was measured by colony formation assay (*C*) and quantitatively analyzed (*D*); representative images shown here are selected from three independent experiments. The scale bar represents 50 μm. *$p < 0.05$; **$p < 0.01$; and ***$p < 0.001$. *E*, cell proliferation was measured with CCK8 assay in HCT116 and HT29 cells with or without eIF3i knockdown. Data represents mean ± SD from three independent experiments. *F*, EdU staining indicates increased cell mitosis activity with eIF3i knockdown using eIF3i -shRNA (sheIF3i), and scrambled shRNA (NT) was used as control. *Left panel*, *green* represents EdU staining for replicated DNA; *blue* represents DAPI staining for cell nucleus; the merged lane shows colocalization. The scale bar represents 50 μm. *G*, quantification (percentage of EdU-positive cells) of the *panel F*. Data represent mean ± SD from at least three independent assays. *$p < 0.05$; **$p < 0.01$; and ***$p < 0.001$. eIF3i, eukaryotic translation initiation factor 3 subunit i; EdU, 5-ethynyl-2′- deoxyuridine; shNT, scrambled control shRNA.

expression as P site serves as the ribosome's second binding site for tRNA, while the uORF represents an ORF located within the 5′UTR of the mRNA. Thus, knockdown of *eIF3i* may hinder the access of ribosomes to the protein-coding ORF, resulting in translation inhibition. The hypothesis is supported by the combined analysis of RNA-seq and Ribo-seq, revealing a substantial decrease in gene translation efficiency upon *eIF3i* knockdown (Fig. S4, *A* and *B*).

Proteomic analysis was conducted on HCT116 cells following *eIF3i* knockdown. principal component analysis demonstrated a significant divergence between the *eIF3i* knockdown group and the control group (Fig. S4C). After knocking down *eIF3i*, the expression of 308 proteins decreased, while the expression of 239 proteins increased (Fig. S4D). Notably, the downregulated proteins were primarily associated with enriched molecular functions in metabolic pathways, translational initiation, and biosynthetic processes (Fig. S4, *E* and *F* and Table S3). Integration of RNA-seq (no change), Ribo-seq (downregulation), and proteomic analysis (downregulation) enabled the identification of four potential genes regulated by eIF3i, notably including PHGDH, a critical rate-limiting enzyme involved in the serine synthesis pathway (Fig. 3A and Table S4). Ribo-seq data revealed a significant

decrease in ribosome binding on PHGDH mRNA following eIF3i knockdown; however, there was no obvious change on ACTB mRNA (Fig. 3B). Further analysis revealed that the mRNA and protein expression between eIF3i and PHGDH were positively correlated in CRC (Fig. 3, *C* and *D*). Similar to eIF3i, PHGDH upregulation was also observed in various tumor tissues including CRC through multiple databases (Fig. S4, *G–I*).

To explore whether eIF3i exclusively fulfills its function in PHGDH translation, independent of its role in transcription, we conducted RT-qPCR and Western blot assays. The findings revealed negligible alterations in PHGDH mRNA levels in eIF3i knockdown HCT116 and HT29 cells, while there was a substantial reduction in PHGDH protein expression (Fig. 3, *E–G*). Together, the
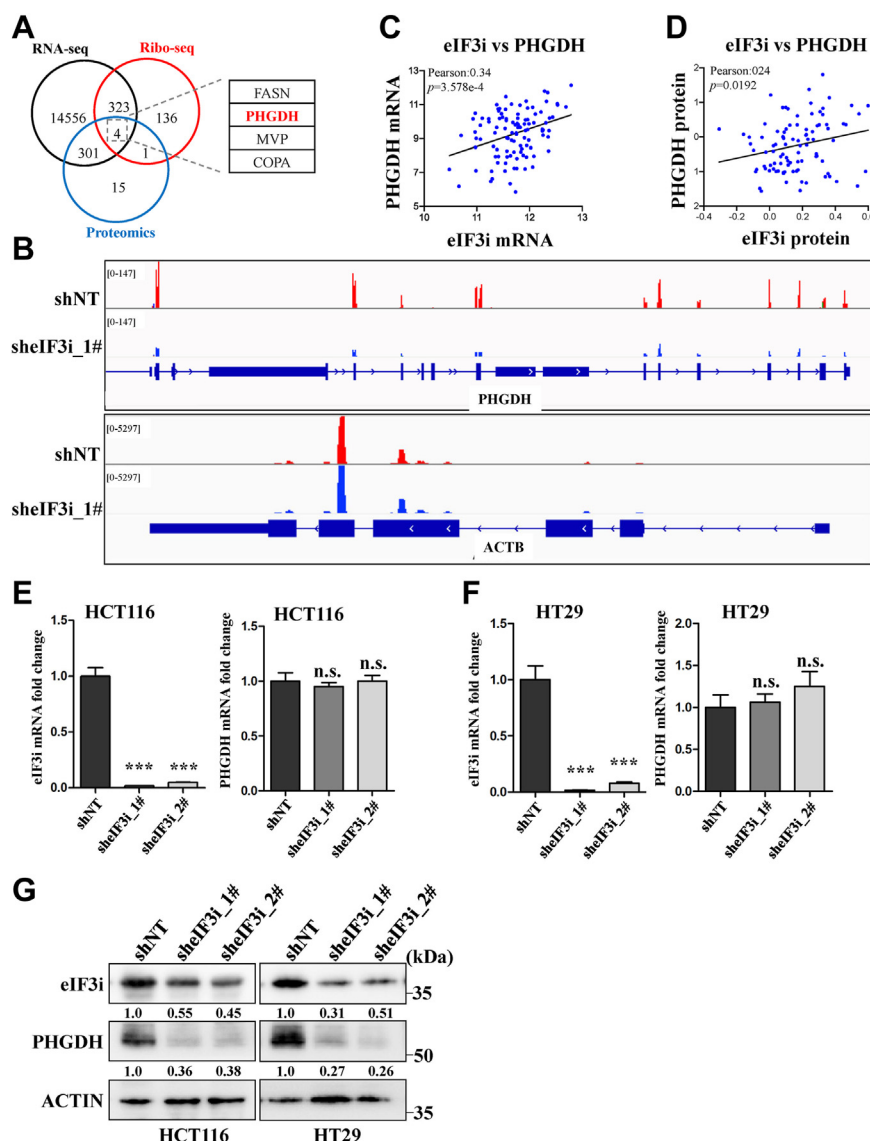

Figure 3. PHGDH is a potential target translationally regulated by eIF3i. *A,* Venn diagram showing potential translational regulatory target genes of eIF3i identified by RNA-seq, Ribo-seq, and proteomics. *B,* representative IGV tracks showed the binding pattern of ribosome on PHGDH and ACTB mRNA after eIF3i knockdown. *C* and *D,* linear regression analyses of mRNA and protein levels between eIF3i and PHGDH, respectively. Pearson correlation coefficients show strong correlation of expression level between eIF3i and PHGDH. Raw data was obtained from cBioPortal database. *E* and *F,* expression of eIF3i and PHGDH mRNA was verified by RT-qPCR analysis after eIF3i knockdown in HCT116 (*E*) and HT29 cells (*F*). ***$p < 0.001$; *n.s.,* not significant. *G,* Western blot analysis shows the protein expression of eIF3i and PHGDH after eIF3i knockdown in HCT116 and HT29 cells. eIF3i, eukaryotic translation initiation factor 3 subunit i; IGV, Integrative Genomics Viewer; PHGDH, D-3-phosphoglycerate dehydrogenase.

above results suggest that PHGDH is a potential target of eIF3i and that eIF3i may be involved in regulating PHGDH translation.

eIF3i–PHGDH axis promotes CRC cell survival

To evaluate the effect of PHGDH on CRC cell proliferation, we employed shRNAs to knockdown *PHGDH* expression
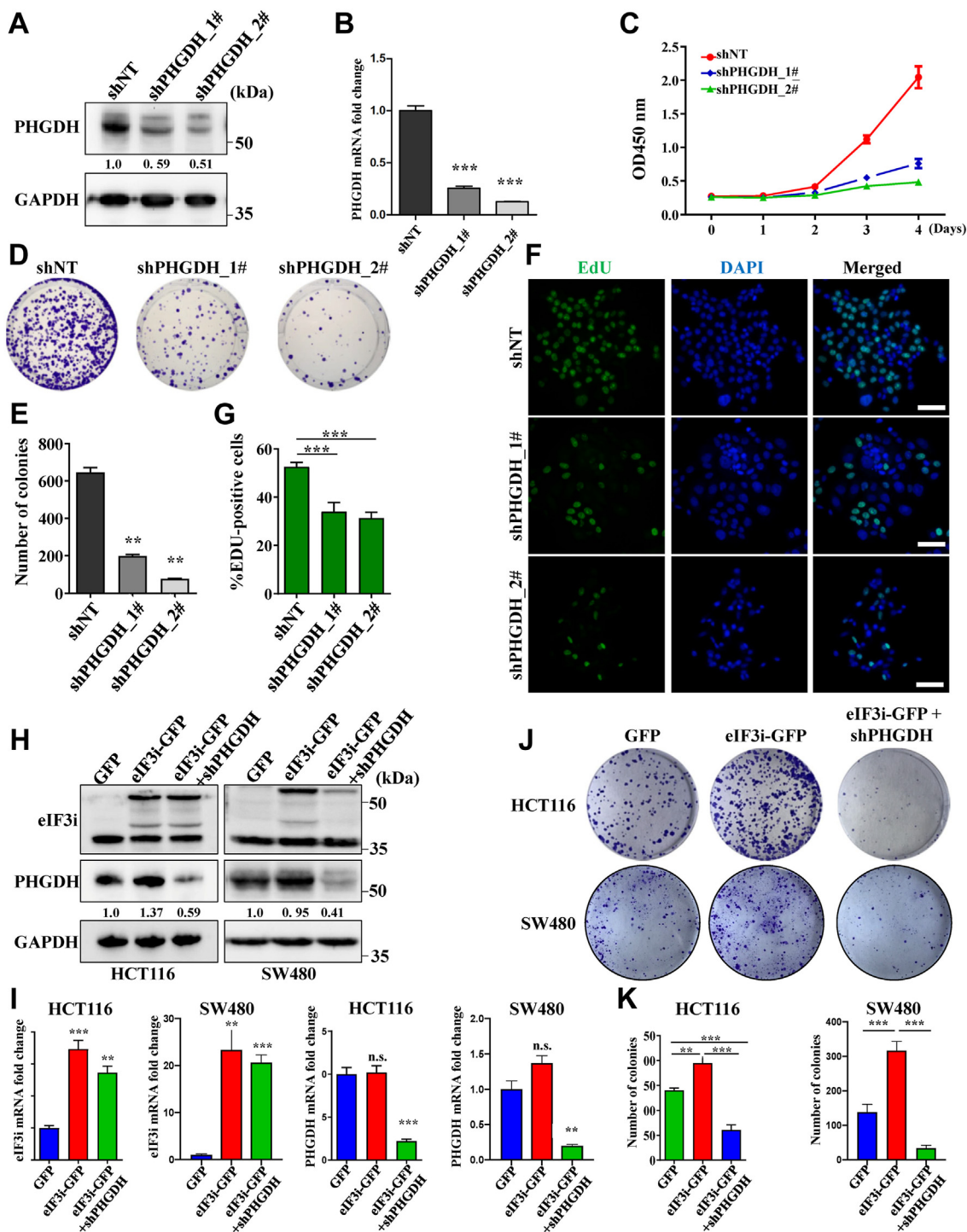
Figure 4. eIF3i–PHGDH axis plays a critical role in CRC cell growth. *A* and *B*, shRNA-mediated PHDGH repression was confirmed by Western blot (*A*) and RT-qPCR (*B*) assays after lentivirus infection in HCT116 cells. ***$p < 0.001$. *C*, CCK-8 assay measures cell proliferation of HCT116 cells after PHGDH knockdown. *D–G*, cell proliferation after PHGDH silencing in HCT116 cells was detected by colony formation assay (*D*) and EdU staining (*F*) and quantitatively analyzed (*E* and *G*) (n = 3 independent experiments). The scale bar represents 50 μm. **$p < 0.01$; ***$p < 0.001$. *H*, PHGDH expression was observed using Western blot analysis after eIF3i overexpression with or without PHGDH repression in HCT116 and SW480 cells. *I*, RT-qPCR analysis showed mRNA expression of eIF3i and PHDGH after eIF3i overexpression with or without PHGDH suppression in HCT116 and SW480 cells. **$p < 0.01$; ***$p < 0.001$; *n.s.*, not significant. *J* and *K*, colony formation assay detected cell proliferation of HCT116 and SW480 cells after eIF3i overexpression and PHGDH knockdown (*J*) and quantitatively analyzed (*K*) (n = 3 independent experiments). **$p < 0.01$; ***$p < 0.001$. CRC, colorectal cancer; CCK-8, Cell Counting Kit-8; eIF3i, eukaryotic translation initiation factor 3 subunit i; EdU, 5-ethynyl-2′- deoxyuridine; PHGDH, D-3-phosphoglycerate dehydrogenase.

(Fig. 4, *A* and *B*). Subsequently, we observed an obvious inhibition in cancer cell proliferation following *PHGDH* knockdown (Figs. 4, *C–E* and S5, *A–D*), providing evidence for the importance of PHGDH in cellular growth. Additionally, the findings from the EdU incorporation assay corroborated these results (Figs. 4, *F* and *G* and S5, *E* and *F*).

As expected, overexpression of eIF3i in HCT116, SW480, and HT29 cells resulted in an obvious increase in PHGDH protein expression (Figs. 4*H* and S5*G*) without changes in its transcription level (Figs. 4*I* and S5*H*). In the meantime, *PHGDH* knockdown suppressed the increase by reducing both RNA transcription and protein expression of PHGDH. These results indicated that eIF3i is involved in the regulation of PHGDH translation instead of transcription (Figs. 4, *H* and *I* and S5, *G* and *H*). Interestingly, the proliferation of HCT116, SW480, and HT29 cells coincided with changes in PHGDH protein expression. Specifically, overexpression of *eIF3i* promoted proliferation, while knockdown of *PHGDH* partially attenuates the excessive growth induced by *eIF3i* overexpression (Figs. 4, *J* and *K* and S5, *I–K*). Conversely, knockdown of *eIF3i* reduced cell proliferation, but overexpressed *PHGDH* could not rescue these phenotypes (Fig. S6, *A–C*). The results support our hypothesis that the restoration of PHGDH mRNA does not alleviate the translation inhibition caused by *eIF3i* defect, indicating a crucial role of eIF3i in the translation of PHGDH protein. Hence, we speculate that PHGDH likely serves as a promising target for eIF3i-mediated translation regulation. Additionally, eIF3i possibly manipulates cell proliferation by facilitating the translation of specific genes including PHGDH.

eIF3i promotes the translation rate of PHGDH

Above findings showed that *eIF3i* overexpression enhances the protein expression of PHGDH without affecting PHGDH mRNA levels (Fig. 4, *H* and *I*). This may be achieved by inhibiting protein degradation or promoting protein translation. To investigate whether eIF3i regulates PHGDH expression by influencing PHGDH protein stability, we employed the protease inhibitor MG132 to assess the stability of PHGDH protein following eIF3i knockdown. The results revealed that MG132 treatment could not rescue the reduction in PHGDH protein expression induced by *eIF3i* knockdown (Fig. S6*D*).

We aimed to investigate whether eIF3i regulates PHGDH expression by controlling PHGDH protein translation. We conducted a polysome assay to examine the impact of eIF3i on the translation rate of PHGDH (Fig. 5*A*). The findings revealed an increase in mRNA level enriched in monosomal following *eIF3i* knockdown, but that in the polysome remarkably decreased (Fig. 5*B*). Importantly, the distribution of rRNA remained largely unchanged following the knockdown of eIF3i, indicating that eIF3i depletion does not impact the distribution of rRNA (Fig. 5*C*). Through sucrose density gradients, we observed strong enrichment of eIF3i and RPS15A in the 40S, 60S, and 80S fractions (Fig. 5*D*). As shown in Figure 5, *E* and *F*, eIF3i knockdown resulted in a predominant shift of PHGDH mRNAs from heavy polysome fractions to light polysome and monosome fractions, while no significant redistribution was observed for ACTB

mRNA. Collectively, these findings strongly suggest that eIF3i regulates the translation rate of PHGDH in CRC cells.

m⁶A modification enhances the PHGDH translation

It is well known that eIF3 is a reader of m⁶A modification. eIF3i acts as a subunit of the eIF3 complex, so we speculate that eIF3i selectively binds to mRNA molecules carrying m⁶A modification, thereby facilitating their translation. To validate this hypothesis, the RNA secondary structure of PHGDH was initially predicted to identify potential m⁶A modification sites. The results showed that the 5′ end of PHGDH mRNA had a shorter and relatively simple secondary structure similar to housekeeping gene ACTB (Fig. S7*A*). Additionally, several potential m⁶A modification sites were observed near the transcription start site of PHGDH mRNA (Fig. S7, *B* and *C*). These findings are consistent with previous results obtained by other researchers through m⁶A-seq, that is, PHGDH mRNA has m⁶A modification at the 5′ end near the transcription start site.

To investigate the necessity of m⁶A modification for eIF3i-mediated PHGDH translation, we used WT and two site mutation (SM) plasmids to perform exogenous PHGDH-GFP expression assays. The PHGDH A127C and A136C sites, located in the coding sequence region of PHGDH, are predicted to be m⁶A sites. In the SM vectors, each adenosine base (A) within predicted m⁶A sites was substituted with cytosine base (C) to abolish the impact of m⁶A methylation, respectively, whereas the m⁶A sites in WT vectors retained intact (Fig. 5*G*). Consistent with expectations, the SM2 group (PHGDH A136C SM) exhibited a significant decrease in GFP protein expression levels and fluorescence intensity compared to both the WT and SM1 groups (PHGDH A127C SM) (Fig. 5, *H–J*). Meanwhile, there was no significant difference in GFP RNA transcription levels (Fig. 5*K*). These results suggest that the m⁶A modification at PHGDH A136 site regulates the translation level of PHGDH mRNA rather than the transcription level.

Next, we investigated the involvement of METTL3, a key writer of m⁶A modifications, in the regulation of PHGDH expression. Although there was no alteration in PHGDH transcription levels (Figs. 6*A* and S8*B*), the absence of *METTL3* resulted in a significant reduction in PHGDH protein (Figs. 6*B* and S8*A*). Moreover, we observed an inhibition of HCT116 and HT29 cell proliferation upon knockdown of *METTL3* (Fig. S8, *C–E*). Importantly, *METTL3* knockdown led to a substantial reduction in the interaction between eIF3i and PHGDH mRNA (Fig. 6, *C* and *D*). This finding suggests the importance of METTL3 for the binding of eIF3i to PHGDH mRNA. Simultaneously, we determined that the stability of PHGDH mRNA remained consistent in both the control and *METTL3* knockdown groups (Fig. 6*E*). However, there was a markedly decrease in the translation rate of PHGDH (Fig. 6, *F* and *G*). Collectively, these findings suggested that METTL3-mediated m⁶A modification promotes the binding of eIF3i to PHGDH mRNA, leading to increased translation without affecting PHGDH mRNA stability.
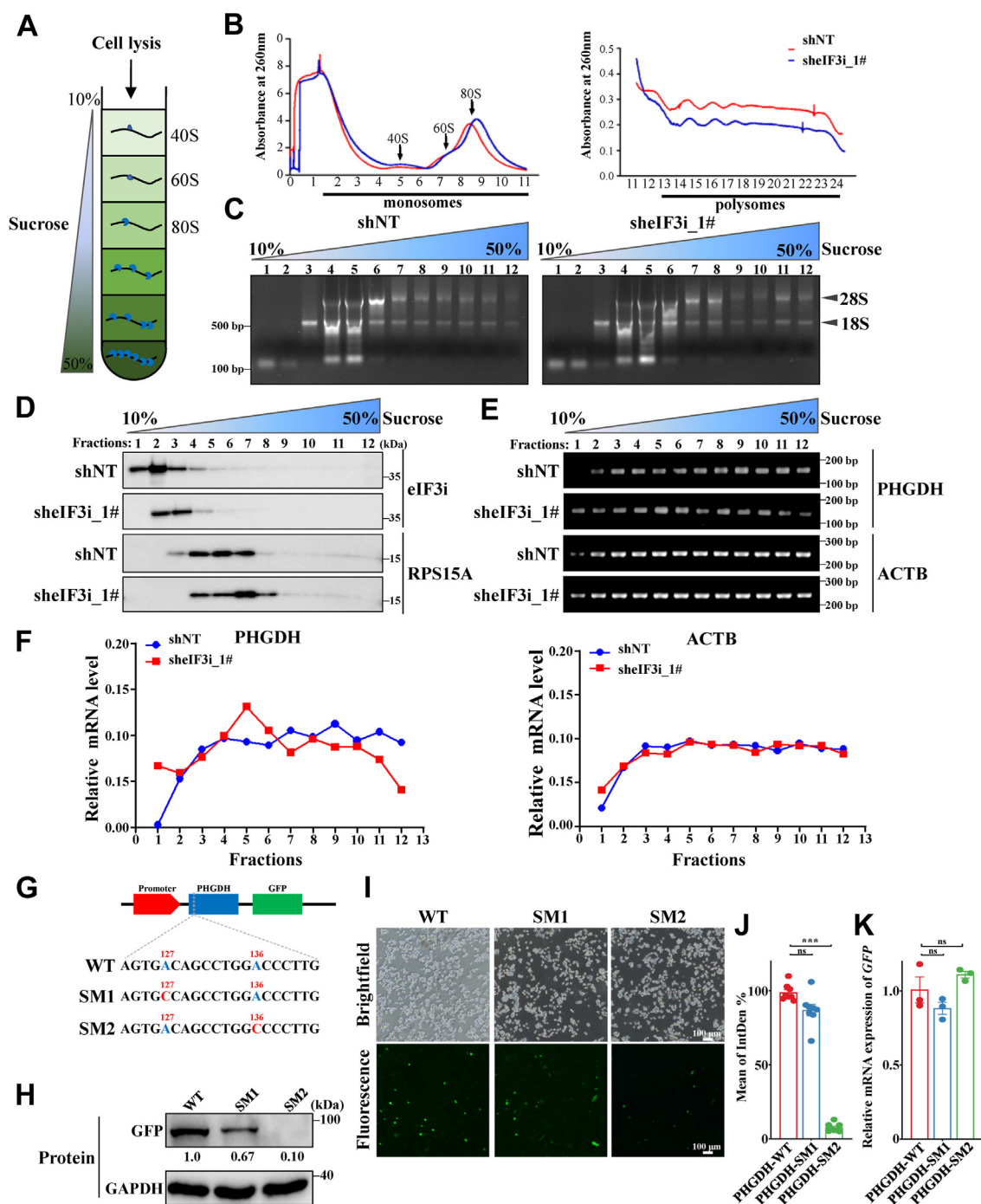
Figure 5. eIF3i promotes PHGDH translation. *A*, schematic diagram of polysome separation by sucrose density gradient. *B*, general polysome profiles in eIF3i knockdown HCT116 cells. *C*, polysomes from shNT and sheIF3i cells were fractionated with sucrose gradients. PHGDH and ACTB RNA in fractions were analyzed by RT-PCR and agarose gel electrophoresis. The *upper panel* shows a schematic diagram of 10 to 50% sucrose gradients, and the *lower panel* shows RNA gel electrophoresis. *D*, the localization of eIF3i and RPS15A proteins in polysomes fractions was identified by Western blot analysis. *E*, PHGDH and ACTB mRNA levels in polysomes fractions in control and sheIF3i cells were analyzed by RT-PCR analysis and subsequent agarose gel electrophoresis. PHGDH mRNA shifts from heavy polysome fractions toward light polysome and monosome fractions in eIF3i knockdown HCT116 cells. *F*, representative images showed PHGDH and ACTB mRNA enrichment in polysomes fractions from control and sheIF3i cells were quantified with ImageJ software (https://imagej.net/software/imagej/). *G*, three PHGDH overexpression plasmids were constructed by inserting the corresponding complementary DNAs into pLenti-control vectors before GFP. WT vectors embodied the PHGDH with intact m⁶A sites, while mutant vectors obtained mono A-C mutations on m⁶A consensus motifs. SM1 contained A127C and SM2 contained A136C mutations, respectively. *H*, GFP expression was identified by Western blotting in HCT116 cells upon transient transfection of PHGDH WT or site mutation vectors. *I*, representative Brightfield (*left*) and GFP fluorescence (*right*) images of HCT116 cells, which were transiently transfected with PHGDH WT or site mutation vectors for 24 h. *J*, quantification of GFP fluorescence from *I*. *K*, GFP expression was identified by qRT-PCR in HCT116 cells upon transient transfection of PHGDH WT or site mutation vectors. ACTB, actin beta; m⁶A,N6-methyladenosine; eIF3i, eukaryotic translation initiation factor 3 subunit i; PHGDH, D-3-phosphoglycerate dehydrogenase.
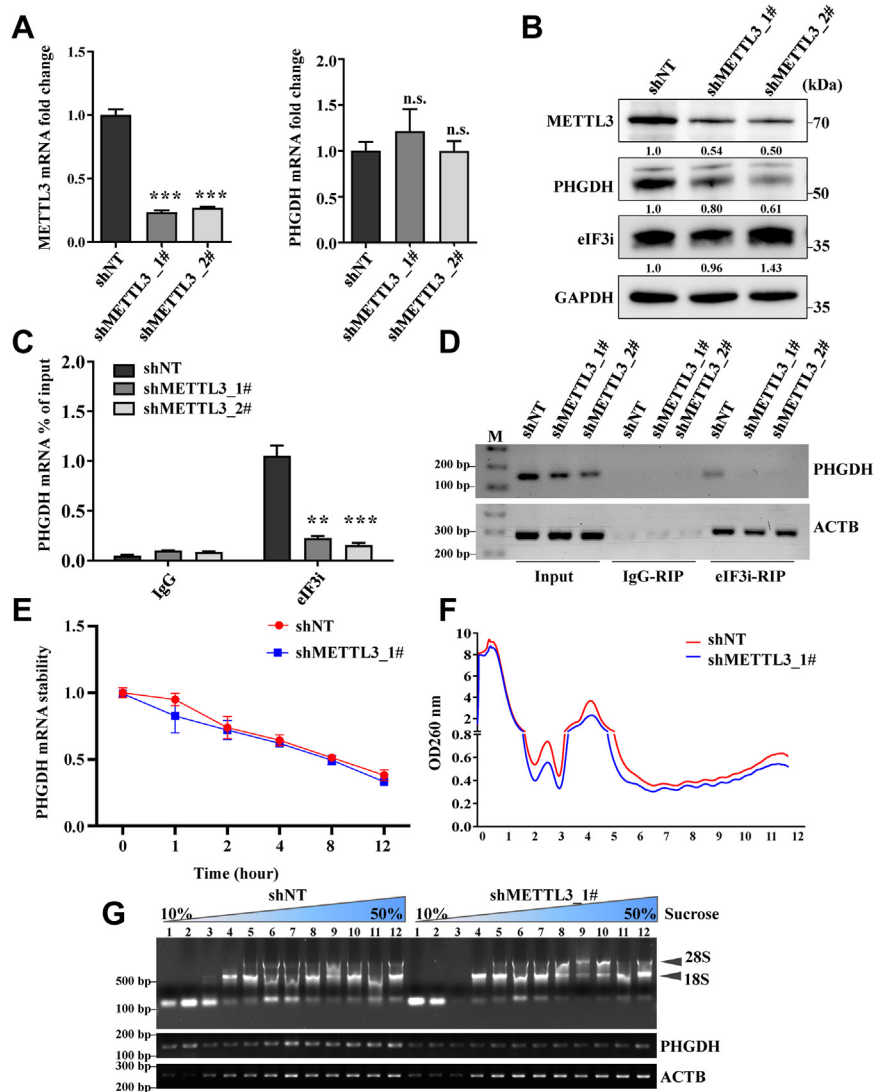
Figure 6. METTL3-mediated m⁶A modification upregulates PHGDH translation. *A*. RT-qPCR analysis of METTL3 and PHGDH mRNA expression after METTL3 knockdown in HCT116 cells. ***$p < 0.001$; *n.s.*, not significant. *B*, Western blot analysis showed protein expression of METTL3, eIF3i, and PHGDH after METTL3 reduction in HCT116 cells. *C*, the binding and interaction relationship between eIF3i protein and PHGDH mRNA with or without METTL3 knockdown was confirmed by eIF3i RIP-qPCR in HCT116 cells (n = 3 independent experiments). **$p < 0.01$; ***$p < 0.001$. *D*, agarose gel electrophoresis detects eIF3i protein enrichment on PHGDH mRNA with or without METTL3 after eIF3i RIP in HCT116 cells. *E*, RT-qPCR analysis detects the stability of PHGDH mRNA after METTL3 knockdown in HCT116 cells (n = 3 independent experiments). *F*, general polysome profiles in METTL3 depletion HCT116 cells. *G*, agarose gel electrophoresis reveals RNA enrichment in polysome fractions. The *upper panel* shows the schematic diagram of 10 to 50% sucrose gradients, the *middle panel* shows the total RNA, and the *lower panels* show the PHGDH and ACTB mRNA after RT-PCR using specific primers. ACTB, actin beta; eIF3i, eukaryotic translation initiation factor 3 subunit i; METTL3, methyltransferase-like protein 3; m⁶A, N6-methyladenosine; PHGDH, D-3-phosphoglycerate dehydrogenase; RIP, RNA-binding protein immunoprecipitation.

## Loss of eIF3i inhibited the growth of xenograft

To assess the regulatory role of eIF3i *in vivo*, we conducted a subcutaneous implantation experiment using nude mice. The results demonstrated a significant reduction in tumor weight and volume among mice derived from tumor cells with suppressed eIF3i or PHGDH expression, as compared to the control groups (Fig. 7, *A* and *B*). Conversely, overexpression of *eIF3i* substantially promoted the growth of transplanted tumors (Fig. 7, *C* and *D*). Moreover, we observed that *PHGDH* knockdown in the *eIF3i*-overexpressing cells partially restrained tumor growth (Fig. 7, *C* and *D*), whereas overexpression of *PHGDH* in *eIF3i*-deficient cells failed to rescue tumor growth (Fig. S8, *F* and *G*). Additionally,

immunohistochemistry results indicated that *eIF3i* knockdown also contributed to reduced PHGDH protein expression *in vivo* (Fig. 7E). Furthermore, either *eIF3i* or *PHGDH* knockdown led to increased apoptosis and decreased proliferation in tumor cells *in vivo* (Fig. 7, *F* and *G*). The above results indicated that eIF3i depletion can inhibit the growth of xenografts most likely *via* attenuating PHGDH translation.

Discussion

The dysregulation of the mRNA translation process has been demonstrated to contribute to tumorigenesis. Tumor cells can hijack protein translation regulation to sustain rapid tumor growth by selectively translating oncogenic transcripts (5). For
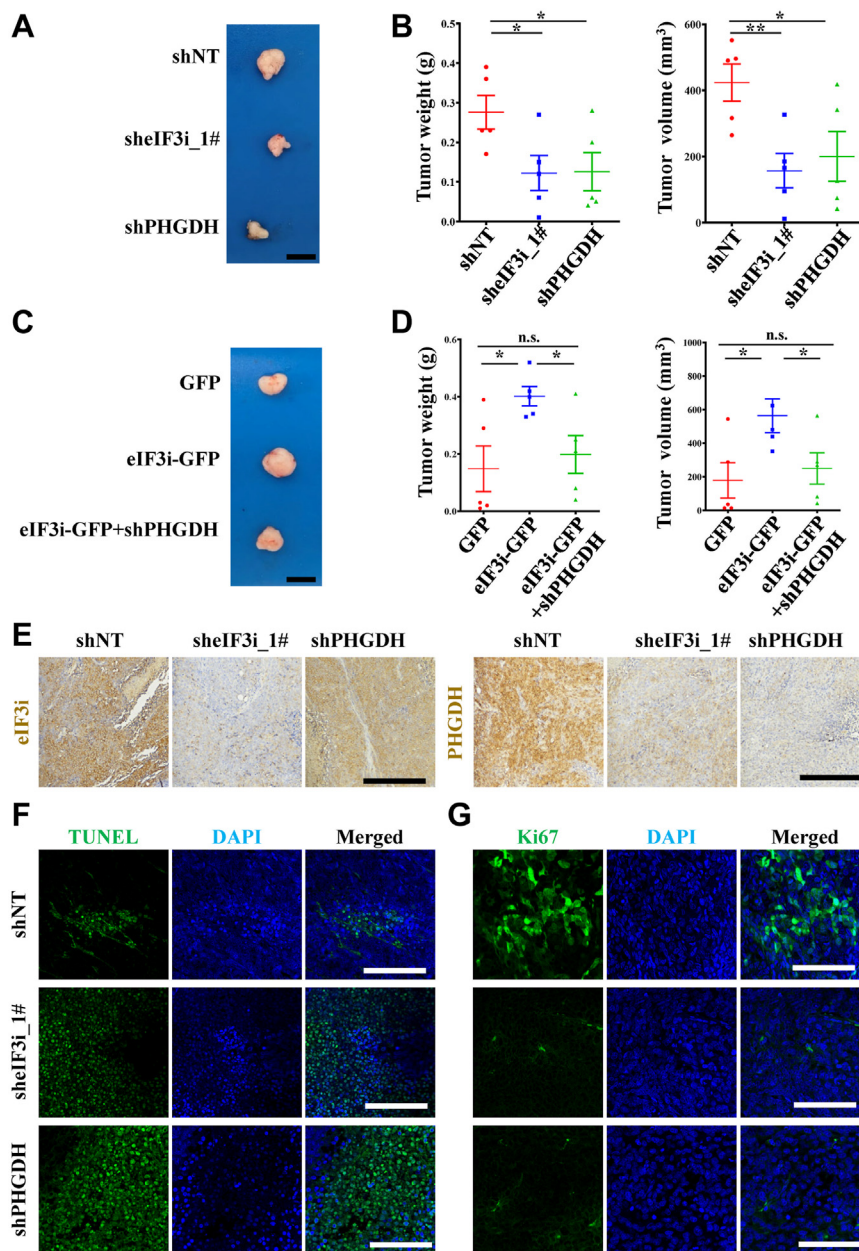
Figure 7. eIF3i and PHGDH depletion impairs xenograft growth. *A*, representative images were subcutaneous tumor models generated by injection of HCT116 cells with eIF3i or PHGDH silencing (n = 5 mice for each group). The scale bar represents 1000 μm. *B*, the statistics of tumor weight (*left*) and volume (*right*) of xenografts in the eIF3i or PHGDH knockdown groups. *$p < 0.05$, **$p < 0.01$. *C*, representative images were subcutaneous tumor models generated by injection of HCT116 control, eIF3i overexpression, and eIF3i overexpression together with PHGDH-silenced group (n = 5 mice for each group). The scale bar represents 1000 μm. *D*, statistics of tumor weight (*left*) and volume (*right*) of xenografts in the control, eIF3i overexpression, and eIF3i overexpression together with PHGDH knockdown group. *$p < 0.05$, *n.s.*, not significant. *E*, IHC analysis presented the eIF3i and PHGDH protein expression in xenograft from (*A*). The scale bar represents 200 μm. *F*, TUNEL assay analyzed the apoptosis levels of xenograft cells in the control, eIF3i-silenced and PHGDH-silenced groups. The scale bar represents 100 μm. *G*, Ki67 staining detects the proliferation of xenografts in the control, eIF3i-silenced and PHGDH-silenced groups. The scale bar represents 100 μm. eIF3i, eukaryotic translation initiation factor 3 subunit i; IHC, immunohistochemistry; PHGDH, D-3-phosphoglycerate dehydrogenase; TUNEL, terminal deoxynucleotidyl transferase–mediated dUTP nick end labeling.

example, while global protein synthesis is suppressed in HeLa cells under hypoxic conditions, the translation efficiency of VEGF mRNA is notably enhanced (32). Under endoplasmic reticulum stress, phosphorylation of eIF2 inhibits the majority of mRNA translation, whereas the subgroup genes regulating crucial functions, such as IBTKα, are preferentially translated (33). In addition, eIF3e enhances the expression of critical regulators associated with cellular stemness by suppressing the expression of stress response proteins in gliomas, thus fostering glioblastoma growth and diminishing tumor cell susceptibility to radiation therapy (34). Our previous studies also found that eIF3i can selectively regulate the translation of VEGF and vascular endothelial growth factor receptor 2, thereby facilitating tumor angiogenesis (18, 22). In this study, we systematically identified potential target genes regulated by eIF3i through multiomics analyses in CRC cells.

Translation in eukaryotes typically initiates at the 5′ end of mRNA through two independent ways: cap-dependent and internal ribosome entry site–dependent. In cap-dependent translation, the 40S ribosomal subunit, assisted by multiple eIFs, attaches to the cap structure located at the 5′ end of mature mRNA. Subsequently, it traverses the 5′ UTR and selectively binds to the start codon. The translation efficiency can be influenced by factors such as the length, secondary structure, and GC content of the 5′ UTR. These factors may alter the interaction between eIFs and the 5′ cap or impede the smooth movement of the ribosome toward the start codon (35, 36). Interestingly, we observed that the PHGDH mRNA possesses a shorter and relatively uncomplicated secondary structure within its 5′ UTR, resembling that of the house-keeping gene ACTB. This characteristic may favorably contribute to its regulation of translation.

Recently, evidence indicates that certain modifications within mRNAs can enhance their translation. These modifications include m^6A (37–39), pseudouridine (Ψ) (40), 5-methylcytidine (39) and ac4C (13, 15). Mechanistically, m^6A primarily (but not exclusively) exerts its effects by recruiting reader proteins (41). The identification of eIF3 as an m^6A reader stems from the observation that eIF3 preferentially binds to m^6A-modified mRNA (42). Among the subunits of the eIF3 complex, eIF3i plays a crucial role. Our findings demonstrate that depletion of *eIF3i* significantly reduces protein translation efficiency, including that of PHGDH. As shown in Figure 3, *E–G*, *eIF3i* depletion inhibits PHGDH protein expression level, while its mRNA level maintains at a constant level. Treatment with the proteasome inhibitor MG132 revealed that this regulation is independent of protein stability (Fig. S6D). Polysome assay unveiled that eIF3i regulates PHGDH expression through translation, as a deficiency of eIF3i leads to a decrease enrichment in polysome distribution on the PHGDH mRNA (Fig. 5, *A–F*). Furthermore, our results indicate that eIF3i promotes PHGDH expression in an m^6A-dependent manner, as a mutation at the PHGDH A136 site markedly inhibits PHGDH protein expression without affecting PHGDH mRNA levels (Fig. 5, *G–K*). Importantly, we discovered that knockdown of the m^6A writer *METTL3* significantly impairs the binding of eIF3i to PHGDH mRNA without affecting mRNA stability, ultimately resulting in attenuated protein synthesis. Our data clearly demonstrated that depletion of either *eIF3i* or *PHGDH* significantly promoted apoptosis, inhibited the growth of CRC cells and xenografts, and contributed to host survival. Although the deletion of *PHGDH* partially inhibits *eIF3i* overexpression–induced proliferation (Figs. 4, *J* and *K*, and 7C), overexpression of PHGDH cannot rescue the decreased proliferation following eIF3i knockdown (Figs. S6, *A–C*, and S8, *F* and *G*). This finding is consistent with our conclusion that eIF3i regulates PHGDH translation. Therefore, the exogenous expression of *PHGDH* has no effect on phenotypes after *eIF3i* knockdown, as it can only be transcribed without undergoing translation. We present the first study demonstrating PHGDH as a direct target of eIF3i in CRC, suggesting that the eIF3i–PHGDH axis may serve as a promising therapeutic target for CRC.

Metabolic reprogramming is recognized as a hallmark of cancer (43). PHGDH, as a key enzyme in the serine synthesis pathway, plays an essential role in remodeling tumor cell metabolism. Recent evidence corroborates our discovery that the loss of PHGDH and subsequent reduction in *de novo* serine biosynthesis leads to the retention of H3K27me3, thereby impeding tumor stem cell differentiation. Furthermore, PHGDH plays a role in regulating tumor growth depending on serine and glycine treatment (44). Moreover, a previous study has shown that glucose deficiency leads to the phosphorylation of PHGDH by p38 at Ser371, which promotes PHGDH translocation from cytosol into nucleus. This, in turn, regulates cell growth *via* poly(ADP-ribosyl)ation of c-Jun (45). Above studies have shown a contradictory function of PHGDH dependent on nutrient treatment or starvation. Moreover, the most recent study has indicated that an interval of reduced PHGDH expression is necessary for the effective metastasis of cancer cells in both primary and metastatic tumors, whereas elevated PHGDH expression promotes their proliferation (46). Thus, PHGDH may be a potential target for cancer therapy and tumor metastasis suppression.

Previous studies have demonstrated that eIF3i could activate β-catenin *via* translational upregulation of cyclooxygenase-2 (17). Additionally, eIF3i is capable of interacting with protein kinase B AKT. Furthermore, the interaction between eIF3i and AKT1 prevents AKT1 dephosphorylation by PP2A, leading to constitutive activation of AKT1 (47). Moreover, PHGDH knockdown leads to a decrease in serine and AKT activity without altering β-catenin levels (48). These findings suggest a correlation between the eIF3i/PHGDH and AKT1/β–catenin signaling pathways. On the other hand, PI3K/AKT pathway activation and MYC proto-oncogene bHLH transcription factor activated by Wnt/β-catenin signaling lead to glucose transporter 1 (GLUT1) overexpression, which is then translocated from the cytoplasm to the plasma membrane and involved in glucose metabolism (49, 50). GLUT1 is essential for the conversion to pyruvate and subsequent metabolization of pyruvate to lactate of cancer cells, thereby enhancing tumor cell migration and invasion (51). Higher expression of GLUT1 increases glucose uptaken and provides substrate for PHGDH-mediated enzymatic reaction (49, 52). Therefore, it is plausible that the AKT1/β–catenin/eIF3i signaling pathways play a beneficial role in PHGDH expression and *de novo* serine synthesis.

Previous studies have shown that p53 (53) and hypoxia-inducible factor (54) regulate the expression of PHGDH at the transcriptional level, and PKCζ (25) and SIRT2 (28) exert their regulatory effects through posttranslational modifications. Nevertheless, the key factors responsible for regulating PHGDH translation and the underlying mechanisms remain unclear to this day. In this study, we have identified PHGDH as a potential target gene for translational regulation by eIF3i using multiomics techniques. Additionally, we have confirmed that eIF3i regulates the translation efficiency of PHGDH in an m^6A-dependent manner. These findings establish a connection between translation regulation and metabolic reprogramming, offering a solid foundation for comprehending the onset and progression of CRC.

Experimental procedures

Cell culture

NCM460, SW480, SW620, HCT116, HT29, and 293T cell lines were purchased from Shanghai Cell Bank and maintained in Dulbecco's modified Eagle's medium (HyClone, AG29629575) supplemented with 10% fetal bovine serum (ExCell Bio, FSP500) and 100 U/ml penicillin/streptomycin (Beyotime, C0222) at 37 °C in a humidified incubator (Thermo Fisher Scientific) with 5% CO_2. These cell lines were verified by short tandem repeats profiling (Supplementary Material).

Plasmid constructions, gene knockdown, and overexpression

Gene knockdown was achieved using the shRNA system. The pLKO.1 vector was digested with AgeI (NEB, R3552) and EcoRI (NEB, R3101). Oligos were synthesized according to the following rules: forward oligo 5′-CCGG-21 bp sense-CTCGAG-21 bp antisense-TTTTTG-3′ and the reverse oligo 5′-AATT-CAAAAA-21 bp sense-CTCGAG-21 bp antisense-3′. The forward oligo and reverse oligo were phosphorylated and annealed and further ligated to the linearized pLKO.1 vector by T4 DNA ligase (NEB, M0202). 293T cells were transfected with pLKO.1-sheIF3i, pLKO.1-shPHGDH, or pLKO.1-shMETTL3 together with packing plasmids psPAX2 and PMD2G. The resulting viral supernatant was used to infect target cells for 24 h. Infected cells were selected with 2 µg/ml puromycin (InvivoGen) for 2 days. Oligo sequences were listed in Table S5.

The human eIF3i gene was amplified from the complementary DNA library of HCT116 cells and cloned into the pLenti-GFP puro vector by the ClonExpress II One Step Cloning Kit (Vazyme, C112-01). GFP was fused to the C terminus of eIF3i *via* a linker (GGS)4. After packaging the virus, SW480 cells were infected and selected by puromycin to obtain a stable GFP-positive eIF3i overexpression cell line. The primers for overexpression plasmids are listed in Table S6.

Immunofluorescence staining assay

For immunofluorescence staining, cells were seeded on slides (WHB, 17175) for 24 h, fixed with 4% paraformaldehyde (Servicebio, G1101), and blocked with 3% bovine serum albumin (BBI, A6600332-0100) supplemented with 0.1% Triton X-100 (Sangon, A110694). Slides were incubated with eIF3i (ProteinTech, 11287-1-AP) or PHGDH (ProteinTech, 14719-1-AP) antibody at 4 °C overnight. After washing with PBS containing 0.1% Triton X-100 buffer three times, slides were incubated in the dark with Alexa Fluor 488–conjugated secondary antibody (Thermo Fisher Scientific, A27034) for 1 h at room temperature. After brief washing, cells were stained with 0.1 µg/ml 4,6-diamino-2-phenyl indole (Solarbio, C0060) in PBS for 10 min at room temperature followed by three washes with PBS containing 0.1% Triton X-100 buffer. The slides were sealed with an antifluorescence quenching reagent (Servicebio, G1401) and subjected to image capture using a confocal microscope (Leica).

IHC analysis

IHC analysis was performed according to a protocol previously reported (55). Briefly, the paraffin sections were deparaffinized, rehydrated, and subjected to antigen retrieval followed by treatment with 3% hydrogen peroxide to block endogenous peroxidase, washing with PBS buffer, blocking in 3% bovine serum albumin for 60 min, and incubation with specific antibodies against eIF3i overnight (ProteinTech, 1:50). After washing three times with PBS buffer, the sections were incubated with biotinylated secondary antibody and SAB tertiary antibody. Finally, sections were stained with 3,3'-diaminobenzidine, counterstained with hematoxylin, dehydrated again, and sealed with neutral balsam. Images were captured using a microscope (Nikon).

Western blot analysis

Whole-cell lysates were prepared in a strong cell lysis buffer (1% SDS, 50 mM Tris–HCl pH 8, 10 mM EDTA, and fresh protease inhibitor cocktail) and ultrasonicated. The cell lysate was quantified, 1 × loading buffer was added, and the cells were boiled for 10 min. Samples were subjected to SDS-PAGE to detect proteins using specific antibodies, including anti-eIF3i (ProteinTech, 1:2000), anti-PHGDH (ProteinTech, 1:2000), and anti-GAPDH (Affinity, 1:5000). Images were captured using a ChemiDoc MP Imaging System (Bio-Rad).

RNA extraction and RT-qPCR

Total RNA was extracted using a Cell Total RNA Isolation Kit (Forgene, RE-03113) according to the manufacturers' protocol. Briefly, after washing once with PBS buffer, cells were lysed by Buffer cRL1 ($<10^6$ cells add 250 µl). Cell lysate was transferred to a DNA-Cleaning Column for centrifugation, and Buffer cRL2 was added to the resulting supernatant (Volume of supernatant: Buffer cRL2 = 1:1.6). The mixture solution was transferred to an RNA-Only Column for centrifugation. After washing the column once with buffer RW1 and twice with RW2, total RNA was eluted with RNase-Free ddH₂O. Reverse transcription was carried out using the PrimeScript RT Master Kit (Takara, RR036A) according to the manufacturer's protocol. Quantitative PCR using novo Start SYBR qPCR SuperMix Plus (Novoprotein, E096-01B) was performed using a CFX96 Real Time PCR System (Bio-Rad). ACTB was used as an internal control to normalize target genes. Primers used in this study are listed in Table S7.

Cell proliferation assay

A total of 2000 cells were seeded in 96-well plates, and Cell Counting Kit-8 (CCK-8, TargetMol, C0005) was added and incubated for 3 h on days 0, 1, 2, 3, and 4 after seeding. The absorbance was measured with a microplate reader (BioTek) at 450 nm.

Colony formation

A total of 2000 cells were seeded in 6-well plates and cultured for 10 to 14 days to form macroscopic clones. The colony was fixed with 4% paraformaldehyde for 20 min, washed twice with PBS buffer, and stained with crystal violet solution at room temperature for 30 min. Colony number was counted after washing with ddH₂O.

EdU incorporation assay

EdU was detected using a Cell-Light Edu Apollo488 *In Vitro* Kit (RiboBio, C10310-3) according to the manufacturers' protocol. Briefly, cells were seeded onto coverslips in 24-well plates at a density of 10,000 cells/well. Twenty-four hours later, the cells were incubated with EdU solution (50 μM) for 2 h and fixed with 4% paraformaldehyde for 30 min. After neutralization with 2 mg/ml glycine solution and washing with PBS buffer, cells were incubated with penetrant (0.5% Triton X-100 in PBS buffer) on a shaker for 10 min. Apollo solution was added and incubated for 30 min in the dark at room temperature. After washing twice with penetrant and methanol, the cells were stained with Hoechst 33342. Slides were sealed with an antifluorescence quenching reagent, and images were captured using a fluorescence microscope (Nikon).

Apoptosis assay

Apoptosis was detected using an Annexin V-FITC/propidium iodide Kit (KeyGen BioTECH) according to manufacturers' protocol. Briefly, cells (shNT, sheIF3i_1#, and sheIF3i_2#) were collected after trypsinization, washed twice with precooled PBS, and resuspended in binding buffer to adjust the cell concentration to 5×10^6/ml. Take 100 μl of cell suspension and add 5 μl of Annexin V/FITC to incubate for 5 min, add 10 μl of propidium iodide and 400 μl of PBS, and then use flow cytometer (Beckman) for detection.

RNA-sequencing

Novogene Bioinformatics Technology Co. performed RNA extraction, library preparation, and RNA-seq. Briefly, control and eIF3i knockdown HCT116 cells were lysed in TRIzol Reagent (Invitrogen, 1559618), and total RNA was extracted according to the manufacturers' protocol. One microgram of RNA per sample was used as input material for preparations. Sequencing libraries were generated using the NEBNext Ultra II RNA Library Prep Kit for Illumina (NEB, E7775) following the manufacturers' protocols, and sequencing was performed on an Illumina HiSeq 2000 platform.

Ribo-sequencing

Ribo-seq was performed as previously described with minor modifications (56). Briefly, cells were fixed with 0.1 mg/ml cycloheximide (Sigma, C7698) and lysed with polysome lysis buffer (10 mM of pH 7.8 Hepes, 150 mM NaCl, 10 mM KCl, 1 mM EDTA, 2 mM MgCl$_2$, 10% glycerol, 0.5% Triton X-100, 1 mM DTT, 0.3 IU/μl RNase inhibitor and protease inhibitor cocktail). The lysate was digested with nucleic acid enzyme, and the ribosome-protected mRNA was separated from free mRNA. The ribosome–mRNA complex was enriched, rRNA was removed and purified with PAGE to obtain the target RNA fragment. Subsequently, the RNA fragments were reverse transcribed to complementary DNA, a sequencing linker was added, and sequencing was performed by Personalbio Co.

Proteomics analysis

Cells were washed with PBS buffer and collected by cell scraping. Cell lysates were prepared with RNA immunoprecipitation (RIP) assay lysis buffer (50 mM Tris–HCl pH 8, 150 mM NaCl, 1% NP-40, 0.5% sodium deoxycholate, 0.1% SDS) for 30 min on ice. After cleaning the lysate at 13,000 rpm for 10 min at 4 °C, the protein concentration was measured using a bicinchoninic acid Protein Concentration Determination Kit (Beyotime, P0012S). Briefly, 50 μg of protein was incubated with iodoacetamide at room temperature for 1 h in the dark. After precipitation with methanol/chloroform, proteins were resuspended in triethylamine bicarbonate buffer. After digestion with trypsin overnight, the resulting peptides were quantified (Thermo Fisher Scientific), and 1 μl of sample was subjected to subsequent experiments. ZipTip (Millipore, ZTC18S096) was activated with 100% acetonitrile and 50% acetonitrile and equilibrated with 1% formic acid. The peptides were adsorbed into Ziptip, desalted with 1% formic acid, and eluted with 50% acetonitrile. The peptides were identified by mass spectrometry.

Polysome assay

Polysome analysis was performed as previously described with minor modifications (18). Briefly, cells were treated with 0.1 mg/ml cycloheximide for 15 min and washed twice with prechilled PBS buffer before collection. Then, the cells were lysed with polysome lysis buffer (10 mM of pH 7.8 Hepes, 150 mM NaCl, 10 mM KCl, 1 mM EDTA, 2 mM MgCl$_2$, 10% glycerol, 0.5% Triton X-100, 1 mM DTT, 0.3 IU/μl RNase inhibitor and protease inhibitor cocktail). The lysate was centrifuged for 10 min at 13,000 rpm and 4 °C. A 10% to 50% sucrose density gradient was prepared by a fully automatic density gradient preparation system (Biocomp). The supernatant was loaded and centrifuged in an ultracentrifuge (Beckman) with a SW40Ti rotor 140,000 G for 3.5 h at 4 °C. The gradients were detected (at 260 nm) and separated by an automatic separation system (Biocomp). The resulting gradients were further divided into 12 fractions, and RNA extraction and RT-PCR analysis were performed.

RIP assay

The RIP assay was performed using a RIP protocol (BersinBio) with minor modifications. We carried out a RIP assay in HCT116 cells with or without METTL3 knockdown to assess and verify the m^{6}A-mediated interaction between eIF3i and PHGDH mRNA. Briefly, cells were harvested and lysed in polysome lysis buffer (10 mM of pH 7.8 Hepes, 150 mM NaCl, 10 mM KCl, 1 mM EDTA, 2 mM MgCl$_2$, 10% glycerol, 0.5% Triton X-100, 1 mM DTT, 0.3 IU/μl RNase inhibitor and protease inhibitor cocktail). After centrifugation, 3 μg of antibodies against rabbit immunoglobulin G or eIF3i were added to the supernatant and incubated overnight at 4 °C. Prewashed protein A/G magnetic beads (Millipore, 16-663) were added to the antibody-sample mixture and incubated at 4 °C for 4 h. After washing the beads three times, RNA was extracted using TRIzol Reagent (Life Technologies, 15596-026). The resulting

RNA was used to analyze PHGDH mRNA using RT-qPCR. Total RNA is used as input.

RNA stability assay

We evaluated the effect of METTL3-mediated m^6A modification on the stability of PHGDH mRNA *via* an RNA decay assay. Briefly, HCT116 cells infected with scramble shRNA or shMETTL3 were cultured in 12-well plates. Actinomycin D (Selleck, S8960) was added to each well to a final concentration of 5 μg/ml. Cells were collected at 0, 30, 60, 120, and 240 min. Total RNA was extracted and subjected to RT-qPCR to quantify the relative abundance of PHGDH mRNA.

Mouse tumor xenograft model

All animal procedures were approved by the local Institutional Animal Care and Use Committee (Approval No. 2021133A). BALB/cA-nu mice were purchased from HFKBio. Eight-week-old female BALB/cA-nu mice were injected subcutaneously with approximately 5×10^6 pretreated HCT116 (three groups, five mice per group) or SW480 (three groups, five mice per group) cells. The mice were sacrificed 4 weeks after injection. Tumor size and weight were measured. The volume of the xenograft was determined using the formula $V = (L \times W^2)/2$.

TUNEL assay

A DeadEnd Fluorometric terminal deoxynucleotidyl transferase–mediated dutp nick end labeling (TUNEL) System Kit (Promega, G3250) was used for the TUNEL assay according to the instruction. Briefly, the tissue sections were deparaffinized in fresh xylene and graded ethanol and fixed by immersing the slides in 4% methanol-free formaldehyde. After washing twice with PBS buffer, proteinase K (20 μg/ml) was added to each slide to cover the tissue section for 10 min at room temperature. Subsequently, the tissue sections were fixed with 4% methanol-free formaldehyde for 5 min. After washing with PBS buffer, the slide was covered with equilibration buffer for a couple of minutes, followed by incubation with Terminal Deoxynucleotidyl Transferase, Recombinant buffer at 37 °C for 1 h in the dark. After terminating the reactions by immersing the slides in 2× saline sodium citrate for 15 min at room temperature followed by washing with fresh PBS buffer three times to remove unincorporated fluorescein-12-2'-deoxyuridine 5'-triphosphate (dUTP), cells were stained with 0.1 μg/ml 4,6-diamino-2-phenyl indole for 10 min at room temperature. The slides were sealed with an antifluorescence quenching reagent, and images were captured using a confocal microscope.

Data analysis using published resources

RNA expression was obtained from GEPIA (57) (http://gepia.cancer-pku.cn/), UALCAN (58) (http://ualcan.path.uab.edu/analysis.html), TIMER2.0 (59) (http://timer.cistrome.org) and The Human Protein Atlas (60) (https://www.proteinatlas.org/). Protein expression was obtained from The Human Protein Atlas (60) (https://www.proteinatlas.org/). The genetic alteration and correlation of gene was obtained from cBio-Portal (61) (http://www.cbioportal.org). The protein structure was obtained from the AlphaFold Protein Structure Database (62) (https://www.alphafold.ebi.ac.uk/). The RNA secondary structure was predicted by the UNAFold Web Server (63) (http://www.unafold.org/). The m^6A modification was predicted by SRAMP (64) (http://www.cuilab.cn/sramp).

Statistical analysis

GraphPad Prism 5 (https://www.graphpad.com/) was used for statistical analysis. Data represent the mean ± SEM, and Student's *t* test was used for all the studies unless otherwise specified. For mouse survival analysis, Kaplan–Meier survival curves were used. $p < 0.05$ was considered a significant difference.

Data availability

All data and materials were available from the corresponding authors on reasonable request.

nick end labeling; uORF, upstream ORF; VEGF, vascular endothelial growth factor; YTHDF, YT521-B homology domain family.

References

1. Sung, H., Ferlay, J., Siegel, R. L., Laversanne, M., Soerjomataram, I., Jemal, A., *et al.* (2021) Global cancer statistics 2020: GLOBOCAN estimates of Incidence and mortality worldwide for 36 cancers in 185 countries. *CA Cancer J. Clin.* **71**, 209–249
2. Salibasic, M., Pusina, S., Bicakcic, E., Pasic, A., Gavric, I., Kulovic, E., *et al.* (2019) Colorectal cancer surgical treatment, our experience. *Med. Arch.* **73**, 412–414
3. Dekker, E., Tanis, P. J., Vleugels, J. L. A., Kasi, P. M., and Wallace, M. B. (2019) Colorectal cancer. *Lancet* **394**, 1467–1480
4. Rosenwald, I. B. (2004) The role of translation in neoplastic transformation from a pathologist's point of view. *Oncogene* **23**, 3230–3247
5. Robichaud, N., Sonenberg, N., Ruggero, D., and Schneider, R. J. (2019) Translational control in cancer. *Cold Spring Harb. Perspect. Biol.* **11**, a032896
6. Micalizzi, D. S., Ebright, R. Y., Haber, D. A., and Maheswaran, S. (2021) Translational regulation of cancer metastasis. *Cancer Res.* **81**, 517–524
7. Lan, Q., Liu, P. Y., Haase, J., Bell, J. L., Huttelmaier, S., and Liu, T. (2019) The critical role of RNA m(6)A methylation in cancer. *Cancer Res.* **79**, 1285–1292
8. Chen, X. Y., Zhang, J., and Zhu, J. S. (2019) The role of m(6)A RNA methylation in human cancer. *Mol. Cancer* **18**, 103
9. Roundtree, I. A., Evans, M. E., Pan, T., and He, C. (2017) Dynamic RNA modifications in gene expression regulation. *Cell* **169**, 1187–1200
10. Jin, D., Guo, J., Wu, Y., Du, J., Yang, L., Wang, X., *et al.* (2019) m(6)A mRNA methylation initiated by METTL3 directly promotes YAP translation and increases YAP activity by regulating the MALAT1-miR-1914-3p-YAP axis to induce NSCLC drug resistance and metastasis. *J. Hematol. Oncol.* **12**, 135
11. Lin, X., Chai, G., Wu, Y., Li, J., Chen, F., Liu, J., *et al.* (2019) RNA m(6)A methylation regulates the epithelial mesenchymal transition of cancer cells and translation of Snail. *Nat. Commun.* **10**, 2065
12. Song, P., Feng, L., Li, J., Dai, D., Zhu, L., Wang, C., *et al.* (2020) β-catenin represses miR455-3p to stimulate m⁶A modification of HSF1 mRNA and promote its translation in colorectal cancer. *Mol. Cancer* **19**, 129
13. Dominissini, D., and Rechavi, G. (2018) N(4)-acetylation of cytidine in mRNA by NAT10 regulates stability and translation. *Cell* **175**, 1725–1727
14. Arango, D., Sturgill, D., Alhusaini, N., Dillman, A. A., Sweet, T. J., Hanson, G., *et al.* (2018) Acetylation of cytidine in mRNA promotes translation efficiency. *Cell* **175**, 1872–1886.e1824
15. Zhang, Y., Jing, Y., Wang, Y., Tang, J., Zhu, X., Jin, W. L., *et al.* (2021) NAT10 promotes gastric cancer metastasis *via* N4-acetylated COL5A1. *Signal. Transduct. Target Ther.* **6**, 173
16. Kolupaeva, V. G., Unbehaun, A., Lomakin, I. B., Hellen, C. U., and Pestova, T. V. (2005) Binding of eukaryotic initiation factor 3 to ribosomal 40S subunits and its role in ribosomal dissociation and anti-association. *RNA* **11**, 470–486
17. Qi, J., Dong, Z., Liu, J., and Zhang, J. T. (2014) EIF3i promotes colon oncogenesis by regulating COX-2 protein synthesis and beta-catenin activation. *Oncogene* **33**, 4156–4163
18. Yuan, Y., Zhang, Y., Yao, S., Shi, H., Huang, X., Li, Y., *et al.* (2014) The translation initiation factor eIF3i up-regulates vascular endothelial growth factor A, accelerates cell proliferation, and promotes angiogenesis in embryonic development and tumorigenesis. *J. Biol. Chem.* **289**, 28310–28323
19. Rauch, J., Ahlemann, M., Schaffrik, M., Mack, B., Ertongur, S., Andratschke, M., *et al.* (2004) Allogenic antibody-mediated identification of head and neck cancer antigens. *Biochem. Biophys. Res. Commun.* **323**, 156–162
20. Xiao, W., Zhang, W., Huang, H., Xie, Y., Zhang, Y., Guo, X., *et al.* (2020) Cancer targeted gene therapy for inhibition of melanoma lung metastasis with eIF3i shRNA loaded liposomes. *Mol. Pharm.* **17**, 229–238
21. Ma, S., Dong, Z., Cui, Q., Liu, J. Y., and Zhang, J. T. (2021) eIF3i regulation of protein synthesis, cell proliferation, cell cycle progression, and tumorigenesis. *Cancer Lett.* **500**, 11–20
22. Zhang, Y., Wang, P., Zhang, Q., Yao, X., Zhao, L., Liu, Y., *et al.* (2017) eIF3i activity is critical for endothelial cells in tumor induced angiogenesis through regulating VEGFR and ERK translation. *Oncotarget* **8**, 19968–19979
23. Zhao, X., Fu, J., Du, J., and Xu, W. (2020) The role of D-3-phosphoglycerate dehydrogenase in cancer. *Int. J. Biol. Sci.* **16**, 1495–1506
24. Labuschagne, C. F., van den Broek, N. J., Mackay, G. M., Vousden, K. H., and Maddocks, O. D. (2014) Serine, but not glycine, supports one-carbon metabolism and proliferation of cancer cells. *Cell Rep.* **7**, 1248–1258
25. Ma, L., Tao, Y., Duran, A., Llado, V., Galvez, A., Barger, J. F., *et al.* (2013) Control of nutrient stress-induced metabolic reprogramming by PKCzeta in tumorigenesis. *Cell* **152**, 599–611
26. Mullarky, E., Mattaini, K. R., Vander Heiden, M. G., Cantley, L. C., and Locasale, J. W. (2011) PHGDH amplification and altered glucose metabolism in human melanoma. *Pigment Cell Melanoma Res.* **24**, 1112–1115
27. Sullivan, M. R., Mattaini, K. R., Dennstedt, E. A., Nguyen, A. A., Sivanand, S., Reilly, M. F., *et al.* (2019) Increased serine synthesis provides an advantage for tumors arising in tissues where serine levels are limiting. *Cell Metab.* **29**, 1410–1421.e1414
28. Wang, C., Wan, X., Yu, T., Huang, Z., Shen, C., Qi, Q., *et al.* (2020) Acetylation stabilizes phosphoglycerate dehydrogenase by disrupting the interaction of E3 ligase RNF5 to promote breast tumorigenesis. *Cell Rep.* **32**, 108021
29. Wei, L., Lee, D., Law, C. T., Zhang, M. S., Shen, J., Chin, D. W., *et al.* (2019) Genome-wide CRISPR/Cas9 library screening identified PHGDH as a critical driver for Sorafenib resistance in HCC. *Nat. Commun.* **10**, 4681
30. Jia, X. Q., Zhang, S., Zhu, H. J., Wang, W., Zhu, J. H., Wang, X. D., *et al.* (2016) Increased expression of PHGDH and prognostic significance in colorectal cancer. *Transl. Oncol.* **9**, 191–196
31. Ma, Y., Zhang, P., Wang, F., Yang, J., Yang, Z., and Qin, H. (2010) The relationship between early embryo development and tumourigenesis. *J. Cell Mol. Med.* **14**, 2697–2701
32. Young, R. M., Wang, S. J., Gordan, J. D., Ji, X., Liebhaber, S. A., and Simon, M. C. (2008) Hypoxia-mediated selective mRNA translation by an internal ribosome entry site-independent mechanism. *J. Biol. Chem.* **283**, 16309–16319
33. Baird, T. D., Palam, L. R., Fusakio, M. E., Willy, J. A., Davis, C. M., McClintick, J. N., *et al.* (2014) Selective mRNA translation during eIF2 phosphorylation induces expression of IBTKalpha. *Mol. Biol. Cell* **25**, 1686–1697
34. Bertorello, J., Sesen, J., Gilhodes, J., Evrard, S., Courtade-Saidi, M., Augustus, M., *et al.* (2020) Translation reprogramming by eIF3 linked to glioblastoma resistance. *NAR Cancer* **2**, zcaa020
35. Kozak, M. (2005) Regulation of translation *via* mRNA structure in prokaryotes and eukaryotes. *Gene* **361**, 13–37
36. Leppek, K., Das, R., and Barna, M. (2018) Functional 5' UTR mRNA structures in eukaryotic translation regulation and how to find them. *Nat. Rev. Mol. Cell Biol.* **19**, 158–174
37. Liu, S., Hausmann, S., Carlson, S. M., Fuentes, M. E., Francis, J. W., Pillai, R., *et al.* (2019) METTL13 methylation of eEF1A increases translational output to promote tumorigenesis. *Cell* **176**, 491–504.e421
38. Liu, T., Wei, Q., Jin, J., Luo, Q., Liu, Y., Yang, Y., *et al.* (2020) The m⁶A reader YTHDF1 promotes ovarian cancer progression *via* augmenting EIF3C translation. *Nucleic Acids Res.* **48**, 3816–3831
39. Li, Q., Li, X., Tang, H., Jiang, B., Dou, Y., Gorospe, M., *et al.* (2017) NSUN2-Mediated m5C methylation and METTL3/METTL14-mediated m⁶A methylation cooperatively enhance p21 translation. *J. Cell Biochem.* **118**, 2587–2598
40. Warren, L., Manos, P. D., Ahfeldt, T., Loh, Y. H., Li, H., Lau, F., *et al.* (2010) Highly efficient reprogramming to pluripotency and directed differentiation of human cells with synthetic modified mRNA. *Cell Stem Cell* **7**, 618–630

41. Wiener, D., and Schwartz, S. (2021) The epitranscriptome beyond m(6)A. *Nat. Rev. Genet.* **22**, 119–131

42. Meyer, K. D., Patil, D. P., Zhou, J., Zinoviev, A., Skabkin, M. A., Elemento, O., *et al.* (2015) 5' UTR m(6)A promotes cap-independent translation. *Cell* **163**, 999–1010

43. Pavlova, N. N., and Thompson, C. B. (2016) The emerging hallmarks of cancer metabolism. *Cell Metab.* **23**, 27–47

44. Baksh, S. C., Todorova, P. K., Gur-Cohen, S., Hurwitz, B., Ge, Y., Novak, J. S. S., *et al.* (2020) Extracellular serine controls epidermal stem cell fate and tumour initiation. *Nat. Cell Biol.* **22**, 779–790

45. Ma, C., Zheng, K., Jiang, K., Zhao, Q., Sha, N., Wang, W., *et al.* (2021) The alternative activity of nuclear PHGDH contributes to tumour growth under nutrient stress. *Nat. Metab.* **3**, 1357–1371

46. Rossi, M., Altea-Manzano, P., Demicco, M., Doglioni, G., Bornes, L., Fukano, M., *et al.* (2022) PHGDH heterogeneity potentiates cancer cell dissemination and metastasis. *Nature* **605**, 747–753

47. Wang, Y. W., Lin, K. T., Chen, S. C., Gu, D. L., Chen, C. F., Tu, P. H., *et al.* (2013) Overexpressed-eIF3I interacted and activated oncogenic Akt1 is a theranostic target in human hepatocellular carcinoma. *Hepatology* **58**, 239–250

48. Ma, X., Li, B., Liu, J., Fu, Y., and Luo, Y. (2019) Phosphoglycerate dehydrogenase promotes pancreatic cancer development by interacting with eIF4A1 and eIF4E. *J. Exp. Clin. Cancer Res.* **38**, 66

49. Shin, E., and Koo, J. S. (2021) Glucose metabolism and glucose transporters in breast cancer. *Front. Cell Dev. Biol.* **9**, 728759

50. Mo, Y., Wang, Y., Zhang, L., Yang, L., Zhou, M., Li, X., *et al.* (2019) The role of Wnt signaling pathway in tumor metabolic reprogramming. *J. Cancer* **10**, 3789–3797

51. San-Millan, I., and Brooks, G. A. (2017) Reexamining cancer metabolism: lactate production for carcinogenesis could be the purpose and explanation of the Warburg Effect. *Carcinogenesis* **38**, 119–133

52. Garrido, P., Moran, J., Alonso, A., Gonzalez, S., and Gonzalez, C. (2013) 17beta-estradiol activates glucose uptake *via* GLUT4 translocation and PI3K/Akt signaling pathway in MCF-7 cells. *Endocrinology* **154**, 1979–1989

53. Ou, Y., Wang, S. J., Jiang, L., Zheng, B., and Gu, W. (2015) p53 Protein-mediated regulation of phosphoglycerate dehydrogenase (PHGDH) is crucial for the apoptotic response upon serine starvation. *J. Biol. Chem.* **290**, 457–466

54. Yoshino, H., Nohata, N., Miyamoto, K., Yonemori, M., Sakaguchi, T., Sugita, S., *et al.* (2017) PHGDH as a key enzyme for serine biosynthesis in HIF2alpha-targeting therapy for renal cell carcinoma. *Cancer Res.* **77**, 6321–6329

55. Hu, X., Meng, Y., Xu, L., Qiu, L., Wei, M., Su, D., *et al.* (2019) Cul4 E3 ubiquitin ligase regulates ovarian cancer drug resistance by targeting the antiapoptotic protein BIRC3. *Cell Death Dis.* **10**, 104

56. Dalley, B. K., Baird, L., and Howard, M. T. (2018) Studying selenoprotein mRNA translation using RNA-seq and ribosome profiling. *Methods Mol. Biol.* **1661**, 103–123

57. Tang, Z., Li, C., Kang, B., Gao, G., Li, C., and Zhang, Z. (2017) GEPIA: a web server for cancer and normal gene expression profiling and interactive analyses. *Nucleic Acids Res.* **45**, W98–W102

58. Chandrashekar, D. S., Karthikeyan, S. K., Korla, P. K., Patel, H., Shovon, A. R., Athar, M., *et al.* (2022) UALCAN: an update to the integrated cancer data analysis platform. *Neoplasia* **25**, 18–27

59. Li, T., Fu, J., Zeng, Z., Cohen, D., Li, J., Chen, Q., *et al.* (2020) TIMER2.0 for analysis of tumor-infiltrating immune cells. *Nucleic Acids Res.* **48**, W509–W514

60. Uhlen, M., Fagerberg, L., Hallstrom, B. M., Lindskog, C., Oksvold, P., Mardinoglu, A., *et al.* (2015) Proteomics. Tissue-based map of the human proteome. *Science* **347**, 1260419

61. Gao, J., Aksoy, B. A., Dogrusoz, U., Dresdner, G., Gross, B., Sumer, S. O., *et al.* (2013) Integrative analysis of complex cancer genomics and clinical profiles using the cBioPortal. *Sci. Signal.* **6**, pl1

62. Varadi, M., Anyango, S., Deshpande, M., Nair, S., Natassia, C., Yordanova, G., *et al.* (2022) AlphaFold Protein Structure Database: massively expanding the structural coverage of protein-sequence space with high-accuracy models. *Nucleic Acids Res.* **50**, D439–D444

63. Zuker, M. (2003) Mfold web server for nucleic acid folding and hybridization prediction. *Nucleic Acids Res.* **31**, 3406–3415

64. Zhou, Y., Zeng, P., Li, Y. H., Zhang, Z., and Cui, Q. (2016) SRAMP: prediction of mammalian N6-methyladenosine (m^{6}A) sites based on sequence-derived features. *Nucleic Acids Res.* **44**, e91

ASBMB